

The Effect of Large-Scale Inhomogeneities on the Luminosity Distance

Nikolaos Brouzakis, Nikolaos Tetradis and Eleftheria Tzavara

University of Athens, Department of Physics, University Campus, Zographou 157 84,
Athens, Greece

Abstract. We study the form of the luminosity distance as a function of redshift in the presence of large scale inhomogeneities, with sizes of order 10 Mpc or larger. We approximate the Universe through the Swiss-cheese model, with each spherical region described by the Lemaitre-Tolman-Bondi metric. We study the propagation of light beams in this background, assuming that the locations of the source and the observer are random. We derive the optical equations for the evolution of the beam area and shear. Through their integration we determine the configurations that can lead to an increase of the luminosity distance relative to the homogeneous cosmology. We find that this can be achieved if the Universe is composed of spherical void-like regions, with matter concentrated near their surface. For inhomogeneities consistent with the observed large scale structure, the relative increase of the luminosity distance is of the order of a few percent at redshifts near 1, and falls short of explaining the substantial increase required by the supernova data. On the other hand, the effect we describe is important for the correct determination of the energy content of the Universe from observations.

1. Introduction

The form of the luminosity distance as a function of redshift for distant supernovae supports the conclusion that the recent expansion of our Universe has been accelerating [1, 2]. In the context of homogeneous cosmology, a recent accelerating phase is also in agreement with the observed perturbations in the cosmic microwave background [3]. The simplest explanation for this phenomenon is that the cosmological constant is non-zero. However, the absence of acceleration at redshifts $z \gtrsim 1$ implies that the required value of the cosmological constant is approximately 120 orders of magnitude smaller than its natural value in terms of the Planck scale.

Various attempts at an alternative explanation try to build a link between inhomogeneities in the matter distribution in the Universe and the perceived cosmological acceleration. For example, there have been arguments, based on perturbative estimates, that the backreaction of super-horizon perturbations on the cosmological expansion is significant and could cause the acceleration [4]. However, the validity of this effect is questionable [5, 6].

We are interested in the importance for the problem of cosmological acceleration of inhomogeneities with sub-horizon characteristic scales today [7]. An intriguing fact is that the accelerating phase coincides with the period in which inhomogeneities in the matter distribution at scales $\mathcal{O}(10) h^{-1}$ Mpc become large, so that the Universe cannot be approximated as homogeneous any more at these scales. Such distances are still small compared to the Hubble distance $\sim 3 \times 10^3 h^{-1}$ Mpc, that sets the scale over which the Universe is assumed to be described by the homogeneous Friedmann-Robertson-Walker (FRW) metric. However, the presence of structures, such as walls or voids, with sizes up to $100 h^{-1}$ Mpc poses the question of whether their influence on the homogeneous solution is substantial.

Because of the significant growth of such inhomogeneities at recent times, a perturbative treatment may not be sufficient. An exact solution of the Einstein equations, even for a simplified geometry, could be more useful in order to reveal an underlying mechanism. The Lemaitre-Tolman-Bondi (LTB) metric [8] has been employed often in this context [9]–[18]. It has been observed that any form of the luminosity distance as a function of redshift can be reproduced with this metric [9]. However, reproducing the supernova data requires a variation of the density or the expansion rate over distances $\mathcal{O}(10^3) h^{-1}$ Mpc [14]–[18]. Moreover, in order to avoid a conflict with the isotropy of the Cosmic Microwave Background (CMB), the location of the observer must be near the center of the spherical configuration described by the LTB metric.

In this work we study the effect of inhomogeneities on the luminosity distance without assuming a preferred location of the observer. We model the inhomogeneities as spherical regions within which the geometry is described by the LTB metric. At

the boundary of these regions, the LTB metric is matched with the FRW metric that describes the evolution in the region between the inhomogeneities. In this way, we model the Universe as consisting of collapsing or expanding inhomogeneous regions, while we preserve the notion of a common scale factor that describes the expansion of the homogeneous intermediate regions. Our model is similar to the standard Swiss-cheese model [19], with the replacement of the Schwarzschild metric with the LTB one. For this reason we refer to it as the LTB Swiss-cheese model.

The transmission of a light beam in such a background can be studied through the Sachs optical equations [20]. These describe the expansion and shear of the beam along its null trajectory. Apart from the case of an FRW background, the optical equations have been derived by Kantowski for a Schwarzschild background in his study of light propagation in the Swiss-cheese model [21]. We derive the equations for a general LTB background. We then use them in order to study light propagation in the LTB Swiss-cheese model. We focus on the modification of the luminosity distance as a function of redshift with respect to the homogeneous FRW case. We investigate which configurations lead to an increase of the luminosity distance, and estimate the magnitude of the effect.

In the following section and in the appendices we derive the optical equations for LTB, FRW and Schwarzschild backgrounds. The expressions for the last two cases are known, but we summarize them for completeness. In section 3 we discuss the particular details of the LTB metric that we use for the description of the spherical regions of the LTB Swiss-cheese model. In section 4 we present numerical solutions for the cosmological evolution of the background metric. In section 5 we discuss light propagation and the modification of the luminosity distance in the inhomogeneous background. In section 6 we estimate the magnitude of this modification. In section 7 we present our conclusions on the possible explanation of the form of the luminosity function in the context of inhomogeneous cosmology.

2. Optical equations and luminosity distance

The proper cross-section area A of a light beam obeys the equation

$$\frac{dA}{d\lambda} = 2\theta A. \quad (2.1)$$

where θ is the expansion of the beam and λ an affine parameter along the null beam trajectory. The symmetric and traceless shear tensor

$$\sigma_{ab} = \begin{pmatrix} \sigma_1 & \sigma_2 \\ \sigma_2 & -\sigma_1 \end{pmatrix} \quad (2.2)$$

describes deformations of the beam. In this work we study light propagation in space-times with spherical spatial symmetry. In such cases, the off-diagonal elements σ_2 of the shear tensor can be set consistently to zero. The reason is that the eigenvalues $\pm\sigma$ of

the shear tensor determine the deformation of a surface along two principal orthogonal axes perpendicular to the light direction. The rate of stretching in these two directions is given by $\theta + \sigma$ and $\theta - \sigma$, respectively. In the case of spherical symmetry, one principal axis always lies on the plane determined by the null geodesic and the center of symmetry and the second perpendicularly to it. It is possible then to choose a reference basis that includes unit vectors along these principal directions. This permits us to set $\sigma_2 = 0$, $\sigma = \sigma_1$.

The optical equations, derived by Sachs [20], determine the evolution of the beam expansion and shear as the light propagates in a background geometry. For completeness, we include a derivation of these equations in appendix A. In appendix B we derive their specific form in various backgrounds that are relevant for our study.

2.1. Lemaître-Tolman-Bondi (LTB) background

Under the assumption of spherical symmetry, the most general metric for a pressureless, inhomogeneous fluid is the LTB metric [8]. It can be written in the form

$$ds^2 = -dt^2 + b^2(t, r)dr^2 + R^2(t, r)d\Omega^2, \quad (2.3)$$

where $d\Omega^2$ is the metric on a two-sphere. The function $b(t, r)$ is given by

$$b^2(t, r) = \frac{R'^2(t, r)}{1 + f(r)}, \quad (2.4)$$

where the prime denotes differentiation with respect to r , and $f(r)$ is an arbitrary function. The bulk energy momentum tensor has the form

$$T_B^A = \text{diag}(-\rho(t, r), 0, 0, 0). \quad (2.5)$$

The fluid consists of successive shells marked by r , whose local density ρ is time-dependent. The function $R(t, r)$ describes the location of the shell marked by r at the time t . Through an appropriate rescaling it can be chosen to satisfy

$$R(0, r) = r. \quad (2.6)$$

The Einstein equations reduce to

$$\dot{R}^2(t, r) = \frac{1}{8\pi M^2} \frac{\mathcal{M}(r)}{R} + f(r) \quad (2.7)$$

$$\mathcal{M}'(r) = 4\pi R^2 \rho R', \quad (2.8)$$

where the dot denotes differentiation with respect to t , and $G = (16\pi M^2)^{-1}$. The generalized mass function $\mathcal{M}(r)$ of the fluid can be chosen arbitrarily. It incorporates the contributions of all shells up to r . It determines the energy density through eq. (2.8). Because of energy conservation $\mathcal{M}(r)$ is independent of t , while ρ and R depend on both t and r .

Without loss of generality we consider geodesic null curves on the plane with $\theta = \pi/2$. The geodesic equations are ($k^i = dx^i/d\lambda$)

$$\frac{dk^0}{d\lambda} + \frac{\dot{R}'R'}{1+f} (k^1)^2 + \dot{R}R (k^3)^2 = 0 \quad (2.9)$$

$$\frac{dk^1}{d\lambda} + 2\frac{\dot{R}'}{R'}k^0k^1 + \left(\frac{R''}{R'} - \frac{f'}{2(1+f)} \right) (k^1)^2 - (1+f)\frac{R}{R'} (k^3)^2 = 0 \quad (2.10)$$

$$\frac{dk^3}{d\lambda} + 2\frac{\dot{R}}{R}k^0k^3 + 2\frac{R'}{R}k^1k^3 = 0. \quad (2.11)$$

One of them can be replaced by the null condition

$$- (k^0)^2 + \frac{R'^2}{1+f} (k^1)^2 + R^2 (k^3)^2 = 0. \quad (2.12)$$

Eq. (2.11) can be integrated to obtain

$$k^3 = \frac{c_\phi}{R^2}. \quad (2.13)$$

The equations for the expansion θ and the shear σ of a beam take the form

$$\frac{d\theta}{d\lambda} = -\frac{1}{4M^2}\rho (k^0)^2 - \theta^2 - \sigma^2 \quad (2.14)$$

$$\frac{d\sigma}{d\lambda} + 2\theta\sigma = \frac{(k^3)^2 R^2}{4M^2} \left(\rho - \frac{3\mathcal{M}(r)}{4\pi R^3} \right), \quad (2.15)$$

while the equation for the beam area can be written as

$$\frac{1}{\sqrt{A}} \frac{d^2\sqrt{A}}{d\lambda^2} = -\frac{1}{4M^2}\rho (k^0)^2 - \sigma^2. \quad (2.16)$$

It is clear from eq. (2.15) that the shear is generated by inhomogeneities, for which the local energy density is different from the average one.

2.2. Friedmann-Robertson-Walker (FRW) background

The FRW metric is a special case of the LTB metric with

$$R(t, r) = a(t)r \quad f(r) = cr^2, \quad c = 0, \pm 1 \quad (2.17)$$

$$\rho = \frac{c_\rho}{a^3(t)} \quad \mathcal{M}(r) = \frac{4\pi}{3}c_\rho r^3. \quad (2.18)$$

The geodesic equations have the solution

$$k^0 = \frac{c_t}{a(t)} \quad (2.19)$$

$$k^1 = \pm \frac{(1+cr^2)^{1/2}}{a(t)^2} \left[c_t^2 - \frac{c_\phi^2}{r^2} \right]^{1/2} \quad (2.20)$$

$$k^3 = \frac{c_\phi}{a^2(t)r^2}. \quad (2.21)$$

The shear can be consistently set to zero as the r.h.s. of eq. (2.15) vanishes.

The equation for the beam area (2.16) is most easily solved if the center of the coordinate system is taken at the location of the beam source. This implies that $c_\phi = 0$ in eq. (2.21). It can be easily checked that the solution of eq. (2.16) for an outgoing beam is

$$A(\lambda) = r^2(\lambda) a^2(t(\lambda)) \Omega_s. \quad (2.22)$$

The constant Ω_s can be identified with the solid angle spanned by a certain beam when the light is emitted by a point-like isotropic source. We point out that, according to eq. (2.1), the beam expansion θ diverges at the location of the point-like source ($r = 0$).

We also obtain

$$\frac{d\sqrt{A}}{d\lambda} = k^1 a \sqrt{\Omega_s} + r \dot{a} k^0 \sqrt{\Omega_s}. \quad (2.23)$$

At the location of the source the second term vanishes, so that

$$\left. \frac{d\sqrt{A}}{d\lambda} \right|_{r=0} = k^1(0) a(t_s) \sqrt{\Omega_s} = \frac{dr}{d\lambda}(0) a(t_s) \sqrt{\Omega_s} = \frac{dt}{d\lambda}(0) \sqrt{\Omega_s}. \quad (2.24)$$

If we normalize the scale factor so that $a(t_s) = 1$ at the time of the beam emission, we recover the standard expression $A = r^2 \Omega_s$ in flat space-time. In the following sections we study light propagation in more general backgrounds. We assume that the light emission near the source is not affected by the large scale geometry. By choosing an affine parameter that is locally $\lambda = t$ in the vicinity of the source, we can set

$$\left. \frac{d\sqrt{A}}{d\lambda} \right|_{\lambda=0} = \sqrt{\Omega_s}. \quad (2.25)$$

This expression, along with

$$\left. \sqrt{A} \right|_{\lambda=0} = 0, \quad (2.26)$$

provide the initial conditions for the solution of eq. (8.17). For isotropic sources, we also expect the beam shear to vanish at the time of emission.

2.3. Schwarzschild background

The metric has the form

$$ds^2 = - \left(1 - \frac{r_s}{r} \right) dt^2 + \left(1 - \frac{r_s}{r} \right)^{-1} dr^2 + r^2 d\Omega^2, \quad (2.27)$$

where $d\Omega^2$ is the metric on a two-sphere and $r_s = \mathcal{M}_0/(8\pi M^2)$ the Schwarzschild radius.

Without loss of generality we consider geodesic null curves on the plane with $\theta = \pi/2$. The geodesic equations are ($k^i = dx^i/d\lambda$)

$$\frac{dk^0}{d\lambda} + \frac{r_s}{r^2} \left(1 - \frac{r_s}{r} \right)^{-1} k^0 k^1 = 0 \quad (2.28)$$

$$\frac{dk^1}{d\lambda} + \left[\frac{r_s}{2} - r \left(1 - \frac{r_s}{r} \right) \right] (k^3)^2 = 0 \quad (2.29)$$

$$\frac{dk^3}{d\lambda} + \frac{2}{r} k^1 k^3 = 0 \quad (2.30)$$

and the null condition

$$- \left(1 - \frac{r_s}{r} \right) (k^0)^2 + \left(1 - \frac{r_s}{r} \right)^{-1} (k^1)^2 + r^2 (k^3)^2 = 0. \quad (2.31)$$

Their solution is

$$k^0 = c_t \left(1 - \frac{r_s}{r} \right)^{-1} \quad (2.32)$$

$$k^1 = \pm \left[c_t^2 - \frac{c_\phi^2}{r^2} \left(1 - \frac{r_s}{r} \right) \right]^{1/2} \quad (2.33)$$

$$k^3 = \frac{c_\phi}{r^2}. \quad (2.34)$$

The equations for the expansion θ and the shear σ of a beam take the form

$$\frac{d\theta}{d\lambda} = -\theta^2 - \sigma^2 \quad (2.35)$$

$$\frac{d\sigma}{d\lambda} + 2\theta\sigma = -\frac{3(k^3)^2}{2} \frac{r_s}{r}, \quad (2.36)$$

while the equation for the beam area can be written as

$$\frac{1}{\sqrt{A}} \frac{d^2 \sqrt{A}}{d\lambda^2} = -\sigma^2. \quad (2.37)$$

2.4. Luminosity distance and redshift

In order to define the luminosity distance, we consider photons emitted within a solid angle Ω_s by an isotropic source with luminosity L . These photons are detected by an observer for whom the light beam has a cross-section A_o . The redshift factor is

$$1 + z = \frac{\omega_s}{\omega_o} = \frac{k_s^0}{k_o^0}, \quad (2.38)$$

because the frequencies measured at the source and at the observation point are proportional to the values of k^0 at these points. The energy flux f_o measured by the observer is

$$f_o = \frac{L}{4\pi D_L^2} = \frac{L}{4\pi} \frac{\Omega_s}{(1+z)^2 A_o}. \quad (2.39)$$

The above expression allows the determination of the luminosity distance D_L as a function of the redshift z . The beam area can be calculated by solving eq. (8.17), with initial conditions given by eqs. (2.25), (2.26), while the redshift is given by eq. (2.38).

In the case of a FRW background, substitution of eq. (2.22) in eq. (2.39) gives the standard expression $D_L^2 = (1+z)^2 r_o^2 a_o^2$, where r_o corresponds to the comoving radial

coordinate of the observer (for the source $r_s = 0$), and a_o to the value of the scale factor at the time of detection of the light signal.

3. Spherical collapse in a LTB background

The inhomogeneous cosmology we consider is a variation of the Swiss-cheese model [19]. Within a homogeneous background, described by a FRW metric, we consider spherical inhomogeneous regions. The metric within each region has a spherical symmetry around its center. In the traditional scenario, the total mass within every region is assumed to be concentrated at the center, so that the relevant metric is the Schwarzschild one. It is well known that the two metrics (FRW and Schwarzschild) can be matched on their common boundary without the appearance of a singular energy density there. The mass parameter of the Schwarzschild metric must be equal to the total energy within a homogeneous region of radius equal to that of the inhomogeneity. The study of light propagation in such a background was pioneered by Kantowski [21] and underlies the broad subject of gravitational lensing [23].

We are interested in light propagation in a background that accounts for the process of gravitational collapse. Our main aim is to examine how the luminosity-redshift relation is modified when the light crosses regions within which the deviation of the matter distribution from homogeneity is time-dependent. Within a FRW background we consider spherical regions where the space-time is described by the LTB metric (2.3). The assumption of spherical symmetry makes the problem tractable. In a realistic scenario we expect deviations from exact spherical symmetry, but the essence of the conclusions should remain unaffected.

The choice of the two arbitrary functions $\mathcal{M}(r)$ and $f(r)$ in eq. (2.3) can lead to different physical situations. The mass function $\mathcal{M}(r)$ is related to the initial matter distribution. The function $f(r)$ defines an effective curvature term in eq. (2.7). We can also interpret $f(r)$ as part of the initial radial velocity of the fluid. We work in a gauge in which $R(0, r) = r$. We parametrize the initial energy density as $\rho_i(r) = (1 + \epsilon(r)) \rho_{0,i}$, with $\rho_i(r) = \rho(0, r)$ and $|\epsilon(r)| < 1$. The initial energy density of the homogeneous background is $\rho_{0,i} = \rho_0(0)$. If the size of the inhomogeneity is r_0 , a consistent solution requires $4\pi \int_0^{r_0} r^2 \epsilon(r) dr = 0$, so that

$$\mathcal{M}(r_0) = 4\pi \int_0^{r_0} r^2 \rho(r) dr = \frac{4\pi}{3} r_0^3 \rho_{0,i}. \quad (3.1)$$

We assume that at the initial time $t_i = 0$ the expansion rate $H_i = \dot{R}/R = \dot{R}'/R'$ is given for all r by the standard expression in homogeneous cosmology: $H_i^2 = \rho_{0,i}/(6M^2)$. Then, eq. (2.7) with $R(0, r) = r$ implies that

$$f(r) = \frac{\rho_{0,i}}{6M^2} r^2 \left(1 - \frac{3\mathcal{M}(r)}{4\pi r^3 \rho_{0,i}} \right). \quad (3.2)$$

The spatial curvature of the LTB geometry is

$${}^{(3)}R(r, t) = -2 \frac{(fR)'}{R^2 R'}. \quad (3.3)$$

For our choice of $f(r)$ we find that at the initial time

$${}^{(3)}R(r, 0) = -6H_i^2 \left(1 - \frac{\mathcal{M}'}{4\pi r^2 \rho_{0,i}} \right) = -6H_i^2 \left(1 - \frac{\rho_i(r)}{\rho_{0,i}} \right). \quad (3.4)$$

Overdense regions have positive spatial curvature, while underdense ones negative curvature. This is very similar to the initial condition considered in the model of spherical collapse [24].

When the inhomogeneity is denser near the center, we have $f(r) < 0$ for $r < r_0$ and $f(r) = 0$ for $r \geq r_0$. It is then clear from eq. (2.7) that, in an expanding Universe with increasing R , the central region will have $\dot{R} = 0$ at some point in its evolution and will stop expanding. Subsequently, it will reverse its motion and start collapsing.

This point becomes clearer if we consider an example with $\epsilon(r) = \epsilon_1 > 0$ for $r < r_m$, and $\epsilon(r) = -\epsilon_1 r_m^3 / (r_0^3 - r_m^3)$ for $r_m < r < r_0$. In the region $r < r_m$ we have $R(t, r) = a(t)r$, $f(r) = -(\epsilon_1 \rho_{0,i} / 6M^2) r^2$ and

$$\left(\frac{\dot{a}}{a} \right)^2 = \frac{1}{6M^2} \frac{(1 + \epsilon_1) \rho_{0,i}}{a^3} - \frac{\epsilon_1 \rho_{0,i}}{6M^2} \frac{1}{a^2}. \quad (3.5)$$

The evolution is typical of a closed homogeneous Universe with curvature proportional to ϵ_1 . For $r > r_m$, the effective curvature term

$$f(r) = -\frac{\epsilon_1 \rho_{0,i}}{6M^2} \frac{r_m^3}{r} \left(\frac{r_0^3 - r^3}{r_0^3 - r_m^3} \right) \quad (3.6)$$

remains negative, but goes to zero with $r \rightarrow r_0$. The shells with $r_m < r < r_0$ stop expanding and eventually collapse, but at progressively later times. The shell with $r = r_0$ expands forever.

We can obtain an analytical expression for the growth of the central overdensity in this simple model. We define the quantity

$$\zeta(t) = \frac{R(t, r_0)/r_0}{R(t, r_m)/r_m} - 1. \quad (3.7)$$

For $0 < \epsilon_1 \ll 1$, the ratio of the energy density within the perturbation to the energy density far from it is given by the factor $(1 + \zeta)^3$. For $\zeta \lesssim 1$ and $t \gtrsim H_i^{-1}$ we find

$$\zeta \simeq \frac{\epsilon_1}{5} \left(\frac{3}{2} H_i t \right)^{2/3}. \quad (3.8)$$

At a time $t_2 \simeq \epsilon_1^{-3/2} H_i^{-1}$ we have $(1 + \zeta)^3 \simeq 2$, which means that the energy density within the perturbation is twice the value in the homogeneous region. The phase of gravitational collapse starts at a time $t_c \simeq 1.5 t_2$. The growth of the perturbation $\sim t^{2/3}$ is in qualitative agreement with the behaviour predicted by the Jeans analysis for adiabatic subhorizon

perturbations in a matter dominated Universe. Our model can be viewed as an exact solution of the Einstein equations that is consistent with the behaviour expected from perturbation theory in the region of its applicability. It also has the same qualitative features as the model of spherical collapse [24].

This simple model has a physical interpretation for $\epsilon_1 < 0$ as well. In this case the central region is an underdensity, surrounded by a shell with density larger than the average. The approximate analytical treatment remains the same as before. The effective curvature term is always positive and goes to zero for $r \rightarrow r_0$. The central region expands faster than the surrounding shell and its density drops faster than the average. On the other hand, the relative shell size shrinks and its energy density grows relative to the average density. We shall study a model with this typical behaviour in the following.

We emphasize that our choice of the functions $\mathcal{M}(r)$ and $f(r)$ is not the only one possible. A general solution of the effective Friedmann equation (2.7) also depends on an arbitrary function $t_B(r)$ that determines the local Big Bang time. This results from the fact that eq. (2.7) can be integrated with respect to t for fixed r . The solution depends on the combination $t - t_B(R)$, with $t_B(r)$ arbitrary. In our model we have set $t_B(r) = 0$. An example of a study of structure formation, exploring the full freedom of the LTB metric, is given in ref. [25].

One final remark concerns the form of the functions $\rho_i(r)$ and $\epsilon(r)$. If they are discontinuous (as in our simple example) the functions $\mathcal{M}'(r)$, $f'(r)$ and $R'(t, r)$ become discontinuous as well. This implies that the metric (2.3), (2.4) also becomes discontinuous. Of course the discontinuity of $\rho_i(r)$ is only an approximation. The realistic physical situation involves a fast variation of the density. However, in order to avoid complications in the interpretation of our results, we always choose continuous functions $\rho_i(r)$ and $\epsilon(r)$ in the following.

4. The model

Our expressions simplify if we switch to dimensionless variables. We define $\bar{t} = tH_i$, $\bar{r} = r/r_0$, $\bar{R} = R/r_0$, where $H_i^2 = \rho_{0,i}/(6M^2)$ is the initial homogeneous expansion rate and r_0 gives the size of the inhomogeneity in comoving coordinates. The evolution equation becomes

$$\frac{\dot{\bar{R}}^2}{\bar{R}^2} = \frac{3\bar{\mathcal{M}}(\bar{r})}{4\pi\bar{R}^3} + \frac{\bar{f}(\bar{r})}{\bar{R}^2}, \quad (4.1)$$

with $\bar{\mathcal{M}} = \mathcal{M}/(\rho_{0,i}r_0^3)$ and $\bar{f} = 6M^2f/(\rho_{0,i}r_0^2) = f/\bar{H}_i^2$, $\bar{H}_i = H_ir_0$. The dot now denotes a derivative with respect to \bar{t} .

The typical cosmological evolution in our model is displayed in figs. 1 and 2. The initial density $\bar{\rho}_i(r) = \rho_i(r)/\rho_0 = 1 + \epsilon(r)$ is constant $\bar{\rho}_i = 1 + \epsilon_1$ in the region $\bar{r} \leq 0.25$, constant $\bar{\rho}_i = 1 + \epsilon_2$ in the region $0.5 \leq \bar{r} \leq 0.75$, and $\bar{\rho}_i = 1$ for $\bar{r} \geq 1$. In the intervals

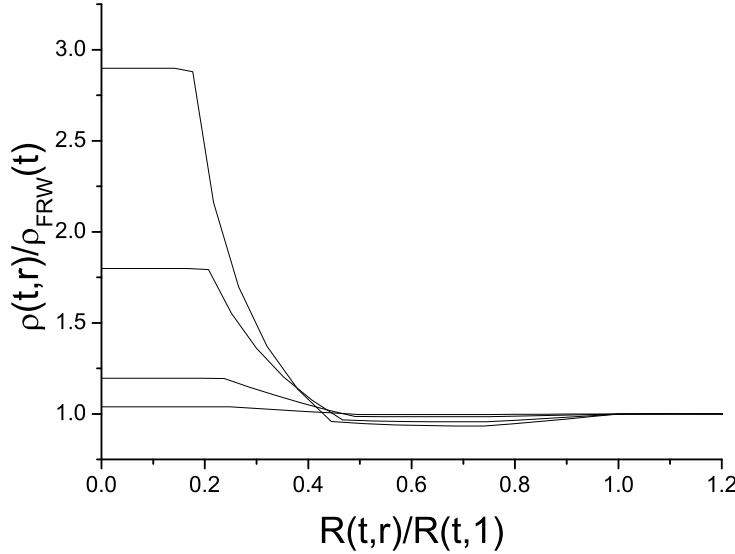


Figure 1. The evolution of the density profile for a central overdensity surrounded by an underdensity.

$0.25 \leq \bar{r} \leq 0.5$ and $0.75 \leq \bar{r} \leq 1$ it interpolates linearly between the values at the boundaries. For fig. 1 we take $\epsilon_1 = 0.01$, while for fig. 2 we use $\epsilon_1 = -0.01$. The values of ϵ_2 are fixed by the requirement that $\int_0^1 \epsilon(r) r^2 dr = 0$.

In fig. 1 we show the typical behaviour in the case of a central overdensity that is surrounded by an underdense region. We display the density profile at times $\bar{t} = 10, 100, 500, 1000$. We normalize the energy density to that of a homogenous FRW background (given by $\bar{\rho}_{FRW}(t) = \bar{\rho}(t, 1)$). The initial time corresponds to the curve with the smallest deviation from 1, while the final to the curve with the largest deviation. We observe that the density contrast grows and eventually becomes $\mathcal{O}(1)$. The central region becomes denser with time, and the underdense region emptier. The central region will stop expanding at a time $\bar{t} \sim 1500$, reverse its motion and collapse towards the center. The same will happen to all the outer shells, but at progressively later times. The shell with $\bar{r} = 1$ expands forever. One important feature is that the relative radius of the central region becomes smaller with time, as the expansion is slower than the average within this region.

In fig. 2 we display the typical behaviour in the case of an underdensity surrounded by an overdense region. We display the density profile at times $\bar{t} = 10, 100, 500, 1000$. As before, the deviation from 1 is smallest at the initial time and largest at the final. The central energy density drops relative to the homogeneous background, while the surrounding region becomes denser. The radius of the central underdensity grows relative

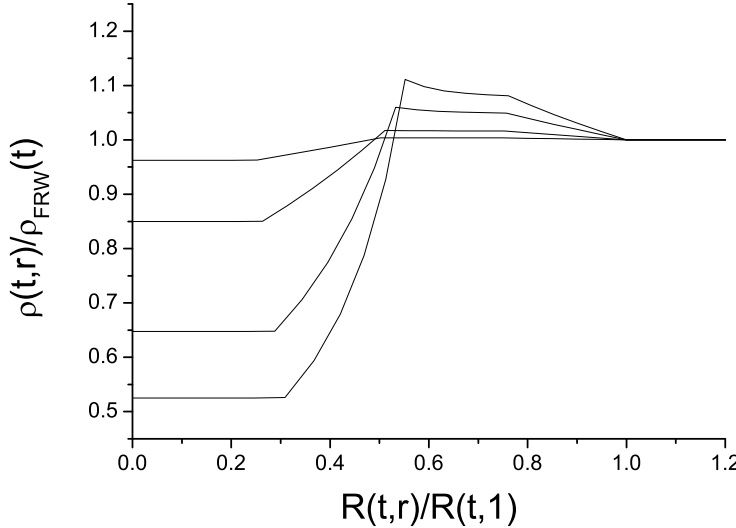


Figure 2. The evolution of the density profile for a central underdensity surrounded by an overdensity.

to the total size of the inhomogeneity, as this region expands faster than the average.

5. Light propagation and luminosity distance

We are interested in light propagation in the gravitational background of the configuration described in the previous section. We take the affine parameter λ to have the dimension of time and we define the dimensionless variables $\bar{\lambda} = H_i \lambda$, $\bar{k}^0 = k^0$, $\bar{k}^1 = k^1/\bar{H}_i$, $\bar{k}^3 = r_0 k^3$. The geodesic equations (2.9)–(2.12) maintain their form, with the various quantities replaced by the barred ones, and the combination $1 + f$ replaced by $\bar{H}_i^{-2} + \bar{f}$. For geodesics going through subhorizon perturbations with $\bar{H}_i \ll 1$ the effective curvature term \bar{f} plays a minor role. However, this term is always important for the evolution of the perturbations, as can be seen from eq. (4.1).

We also define the dimensionless expansion $\bar{\theta} = \theta/H_i$ and shear $\bar{\sigma} = \sigma/H_i$. The optical equations (2.14)–(2.16) take the form

$$\frac{d\bar{\theta}}{d\bar{\lambda}} = -\frac{3}{2}\bar{\rho}(\bar{k}^0)^2 - \bar{\theta}^2 - \bar{\sigma}^2 \quad (5.2)$$

$$\frac{d\bar{\sigma}}{d\bar{\lambda}} + 2\bar{\theta}\bar{\sigma} = \frac{3}{2}(\bar{k}^3)^2 \bar{R}^2 \left(\bar{\rho} - \frac{3\bar{\mathcal{M}}(\bar{r})}{4\pi\bar{R}^3} \right), \quad (5.3)$$

$$\frac{1}{\sqrt{A}} \frac{d^2\sqrt{A}}{d\bar{\lambda}^2} = -\frac{3}{2}\bar{\rho}(\bar{k}^0)^2 - \bar{\sigma}^2, \quad (5.4)$$

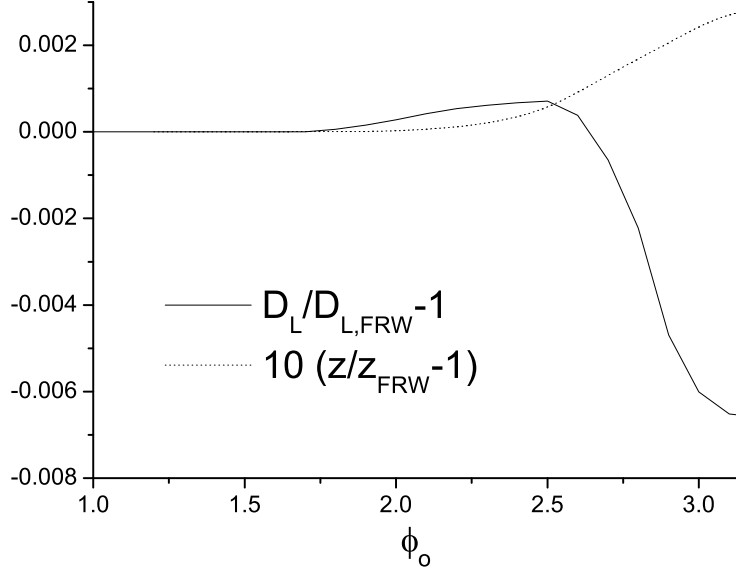


Figure 3. The luminosity distance D_L , relative to the case of homogeneous cosmology, for light beams crossing a configuration with a central overdensity and exiting at various angles ϕ_o .

with $\bar{\rho} = \rho/\rho_{0,i}$. The initial conditions (2.25), (2.26) become

$$\left. \frac{d\sqrt{\bar{A}}}{d\bar{\lambda}} \right|_{\bar{\lambda}=0} = \frac{1}{\bar{H}_i} \sqrt{\bar{\Omega}_s} = \sqrt{\Omega_s}. \quad (5.5)$$

$$\left. \sqrt{\bar{A}} \right|_{\bar{\lambda}=0} = 0, \quad (5.6)$$

with $\bar{A} = H_i^2 A$ and $\bar{\Omega} = \bar{H}_i^2 \Omega$.

For our study we integrate the geodesic and optical equations numerically in the backgrounds described in the previous section. In order to get a feeling of the qualitative effect on the luminosity distance, we consider first a light beam that crosses one spherical inhomogeneous region. We assume that the light is emitted at a radius $\bar{r} = 1.5$. Its trajectory is obtained by integrating eqs. (2.9), (2.11), (2.12) (in their rescaled form). Eq. (2.10) is then automatically satisfied. The initial value of \bar{k}_0 is arbitrary, as it corresponds to the initial frequency of the emitted light. The integration of eq. (2.11) gives eq. (2.13). The angle of entry of the beam into the inhomogeneous region can be varied through the choice of c_ϕ , or its rescaled version $\bar{c}_\phi = c_\phi/r_0$. For $c_\phi = 0$ the trajectory goes through the center of the spherical configuration.

The form of the various light trajectories is not particularly illuminating. The important effect is the difference in light propagation within an inhomogeneous

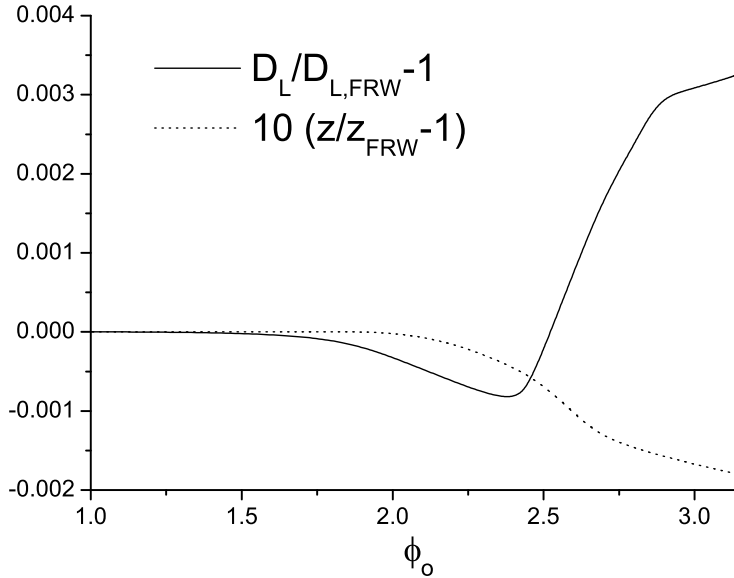


Figure 4. The luminosity distance D_L , relative to the case of homogeneous cosmology, for light beams crossing a configuration with a central underdensity and exiting at various angles ϕ_o .

background and a homogeneous one. In order to make this comparison we consider two light trajectories (one in each background) that start at a common point with $\bar{r} = 1.5$ and eventually approach another common point with $\bar{r} = 1.5$. The value of \bar{c}_ϕ and the length of trajectories in terms of the affine parameter or the coordinate time are different. However, both light beams are emitted and received by comoving observers in the homogeneous region, with the same spatial coordinates. The difference in beam area and redshift is generated by the background that the beam crosses. Alternatively, one could choose to compare beams emitted at the same point within the homogeneous region, with the same c_ϕ . These would approach $\bar{r} = 1.5$ at different values of the angular coordinate ϕ . This choice gives very similar results to the ones we describe.

In figs. 3, 4 we display the difference in luminosity distance and redshift between inhomogeneous and homogeneous backgrounds, as a function of the comoving angle ϕ_o of the observer. The light is emitted from the point $\bar{r}_s = 1.5$, $\phi_s = 0$, and observed at the point $\bar{r}_o = 1.5$, ϕ_o . We have used $\bar{H}_i = 1$ and taken the emission time of the beam to be $\bar{t}_s = 550$. The background within which the light propagates is not consistent with the theory of structure formation, as it includes a perturbation of horizon size with $|\epsilon_1| = 0.01$, instead of the standard $|\epsilon_1| = 10^{-5}$. We choose such a background in order to make its qualitative effect on the beam properties more visible. In the following section, in which

we focus on a quantitative estimate of the effect, we consider realistic backgrounds.

For the results displayed in fig. 3 the inhomogeneity consists of a central overdensity surrounded by an underdensity. For small values of ϕ_o the light trajectory stays within the homogeneous region $1 \leq \bar{r} \leq 1.5$. As a result no difference is observed. For larger angles the trajectory crosses only the underdense part of the inhomogeneity. The resulting luminosity distance is larger than the one for a homogeneous background. At even larger angles the beam enters the central overdense region. The luminosity distance becomes smaller than the one in a homogeneous background. This behaviour is a consequence of the term $\sim \rho(k^0)^2$ in the r.h.s. of eq. (2.16). If the effect is averaged over angles, a decrease of the luminosity distance is expected.

The shear σ has only a minor effect in the evolution of \sqrt{A} and the determination of the luminosity distance. The reason is that the shear is generated by the difference of the local energy density ρ and an average density $\rho_{av} = \mathcal{M}/(4\pi R^3/3)$. These coincide within the central homogeneous region. They are different in the surrounding underdense region. However, the later gives an effect only for beams that stay within the overdensity a short time, without significant modification of the respective luminosity distance. A significant effect can be generated if the mass of the overdensity is concentrated near the center. In this case, eqs. (2.14)-(2.16) give an effect similar to that of eqs. (2.35)-(2.37) for a Schwarzschild geometry, with the additional influence of the expansion. It is known that for a Schwarzschild geometry the shear plays a minor role, unless the beam approaches the center at distances comparable to the Schwarzschild radius [21].

The relative difference in redshift is more than an order of magnitude smaller than the respective difference in luminosity distance. The reason is that the redshift, as opposed to the beam area, receives compensating contributions when entering and exiting the inhomogeneity. The net effect depends only on the evolution with time of the inhomogeneity (the reflection of the Rees-Sciama effect [26] in our formalism), and would be zero for a static one. We conclude that it is a good approximation to assume that the redshift remains unaffected by the presence of the inhomogeneity. This conclusion is consistent with the results of the study based on the standard Swiss-cheese model, in which the inhomogeneous region is modelled through the Schwarzschild geometry [21].

In fig. 4 we display the modification of the luminosity distance and redshift in the case of central underdensity surrounded by an overdensity. Again, we have used $\bar{H}_i = 1$ and taken the emission time of the beam to be $\bar{t}_s = 550$. We observe an effect on the luminosity distance that is opposite to that in the previous case of a central overdensity. Again, the modification of the redshift can be neglected in a good approximation.

The comparison of figs. 3 and 4 demonstrates that the average modification of the luminosity distance, for a large statistical sample of light beams crossing the inhomogeneity at various angles, depends on the form of the configuration. The presence of underdense central regions, consistent with the appearance of large, approximately

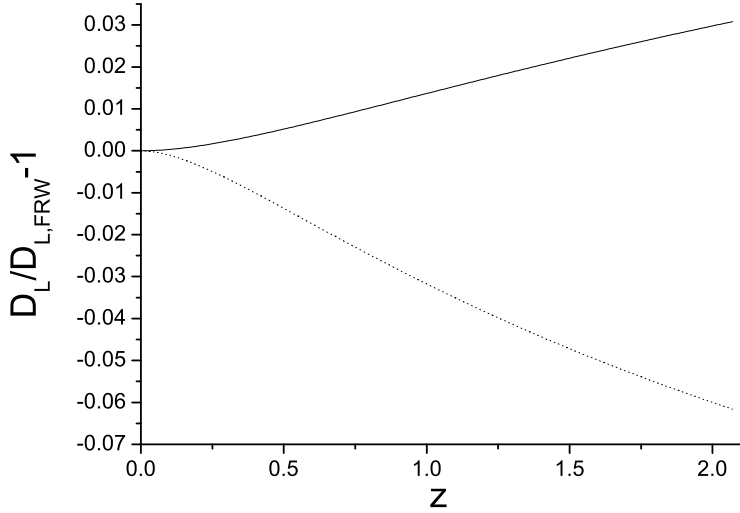


Figure 5. The luminosity distance D_L relative to the case of homogeneous cosmology, as a function of the redshift z , for light beams crossing diametrically several configurations with a central underdensity (upper curve) or overdensity (lower curve).

spherical voids in the matter distribution of the Universe, is expected to lead to an increase of the average luminosity distance relative to the homogeneous case. The opposite is expected if the central regions are overdense. It must be emphasized that the average density is equal to that of the homogeneous case for both configurations displayed in figs. 1 and 2. In this sense, these configurations do not have to appear in equal numbers in a realistic model of the Universe. It seems reasonable to suggest that the dominance of voids, as deduced from observations [22], can be linked with increased luminosity distances.

6. The magnitude of the effect

The important question is whether the dominance of configurations with central underdensities can induce an effect that would explain the observed luminosity curves for distant supernovae. Our model is too basic to address this question in full detail. However, we can use it in order to estimate the magnitude of the expected effect in the real Universe.

The biggest increase in the luminosity distance relative to a homogeneous cosmology is obtained if the Universe includes only void-like inhomogeneities with central underdensities. The effect is maximized if the light is assumed to cross these configurations passing through their center. The effect of the evolution of the inhomogeneities must be taken into account, with initial conditions consistent with the CMB spectrum (amplitude

$\mathcal{O}(10^{-5})$ at horizon crossing) and the observed matter distribution today. Within our model, this can be achieved by using as initial condition a configuration with $\epsilon_1 = -0.01$ and size relative to the horizon $r_0 H_i = \bar{H}_i = 1/10$ at some initial time $\bar{t}_i = 0$. This evolves similarly to fig. 2 into a configuration with a density contrast $\mathcal{O}(1)$ at a time $\bar{t}_f \simeq 1436$, which we identify with the present. The size of the inhomogeneity relative to the horizon today is $R(t_f, r_0) H_f = \dot{R}(t_f, r_0) = \dot{\bar{R}}(\bar{t}_f, 1) \bar{H}_i$. Our solution gives $\dot{\bar{R}}(\bar{t}_f, 1) \simeq 0.076$, so that the size of the inhomogeneity becomes $R(t_f, r_0) \simeq 23 h^{-1}$ Mpc. This is of the order of the typical size of voids today. At times before the initial moment \bar{t}_i from which we follow the evolution, the inhomogeneity is only a small perturbation, with amplitude $\mathcal{O}(10^{-5})$ at horizon crossing.

We consider light beams that pass repeatedly through the inhomogeneities we described above. The light is emitted at some time $\bar{\tau}_s$ from a point with $\bar{r} = 1.5$ within the homogeneous region. The initial conditions for the beam area are given by eqs. (2.25), (2.26). We assume that the light moves radially towards the center of the inhomogeneity (that has a fixed radius $\bar{r}_0 = 1$ in comoving coordinates), exits from the opposite side and finally arrives at a point with $\bar{r} = 1.5$. Subsequently, the beam crosses the following inhomogeneity in a similar fashion. The initial conditions are now set by the values of \sqrt{A} and $d\sqrt{A}/d\bar{\lambda}$ at the end of the first crossing. Our assumption that the motion is radial produces the maximum effect. In general the crossing should take place at a random angle, with a smaller total increase of the luminosity distance. Of course, as time passes the profile of the inhomogeneities changes, as depicted in fig. 2.

The total number of crossings determines the total redshift of the beam and the final beam area, related to the luminosity distance. We repeat the calculation for several starting times that result in a variation of the total number of crossings. In fig. 5 (upper curve) we depict the resulting increase in the luminosity distance relative to the homogeneous case, as a function of the redshift. As we discussed in the previous section, the value of the redshift is essentially unaffected by the presence of the inhomogeneities. (The effect is smaller by more than an order of magnitude compared to the modification of the luminosity distance.) In fig. 5 we also depict the form of the luminosity curve if the inhomogeneity has a central overdensity (lower curve). In this case the luminosity distance is decreased relative to the homogeneous case.

It is clear from fig. 5 that the influence of inhomogeneities on the luminosity distance is a small effect, at most of the order of a few %. This must be compared to the required increase in the luminosity distance in order to explain the supernova data, which is of the order of 30% at redshifts around 1. This conclusion remains valid for other profiles of the inhomogeneities, as long as the essential phenomenological requirements are satisfied (consistency with the observed large scale structure today, amplitude $\mathcal{O}(10^{-5})$ at horizon crossing).

It must be pointed out that the region of validity of our model does not extend to

very high redshifts. Despite the fact that the amplitude of the perturbation goes to zero at early times in our model, a significant increase of the luminosity distance is predicted even for large z . We do not expect such a phenomenon to prevail in a model that preserves the full spectrum of perturbations, instead of keeping only one with a characteristic scale, as we did.

Obtaining an analytical estimate of the modification of the luminosity distance is not easy. However, an absolute upper bound can be derived from eq. (2.16). The “focusing” of a beam is minimized if the shear is negligible and the energy density of the cosmological medium is set to zero in this equation. In our model this idealized situation can be achieved if the central underdense regions of the inhomogeneities become totally empty after a long evolution, while overdense spherical thin shells develop around them. The effect of a shell, no matter how thin, on the beam area is not necessarily negligible. However, if we want to derive only an upper bound on the increase of the luminosity distance, we can set the energy density arbitrarily to zero in the optical equation only. Of course, the energy density still drives the cosmological expansion through eq. (2.7). The scale of the overall expansion is determined by the average energy density. In our model this is obvious from the expansion in the homogeneous regions outside the inhomogeneities.

The equation that we derive in this way corresponds to the partially filled beam equation in FRW cosmology [27, 28], if all the matter is assumed to be concentrated in dense objects that are not crossed by the light trajectories. The same equation results from the optical equation (2.37) within the holes of the standard Swiss-cheese model if the shear is neglected. The luminosity distance as a function of the redshift can be derived analytically in this case, assuming that the background expansion is given by the standard Friedmann equation involving the average density [29]. When comparing it to the luminosity distance in a homogenous matter-dominated FRW cosmology, we find

$$\frac{D_L}{D_{L,FRW}} - 1 = \frac{1}{5} \frac{(1+z)^2 - (1+z)^{-3/2}}{1+z - (1+z)^{1/2}} - 1. \quad (6.7)$$

For redshifts near 1, this expression gives an increase in the luminosity distance by around 10%. This is the maximum effect we could expect, if the expansion rate is governed by the average density through the standard Friedmann equation.

7. Summary and conclusions

The purpose of this study has been to determine the modification of the luminosity distance of astrophysical objects, such as supernovae, which is generated by the appearance of large scale inhomogeneities. We constructed a picture different from that of the standard Swiss-cheese model. The inhomogeneities are still modelled as spherical regions within a homogeneous background, but the matter inside them is not concentrated in very dense objects at their center. Instead, it is continuously distributed in regions of density

below or above the average one. We assumed spherical symmetry for each one of the inhomogeneous configurations. The LTB metric gives the most general description within each spherical region if the cosmological fluid is assumed to be pressureless. Moreover, it provides an automatic matching with the intermediate homogeneous regions, as the FRW metric is a special case of the LTB one. As a result, our model automatically becomes an exact solution of the Einstein equations.

One fundamental assumption in our study was that neither the light source nor the observer occupy a preferred position in the Universe. For this reason we assumed that the light is emitted and received within homogeneous regions, while it crosses one or many inhomogeneous ones along its path. We derived the necessary optical equations that describe the propagation of a light beam within a LTB background.

The cosmological evolution within each spherical region has many realistic elements when compared with the Universe at scales around and above $10 h^{-1}$ Mpc. Central overdense regions become denser with time, with underdense spherical shells surrounding them. Central underdense regions turn into voids, surrounded by massive shells. The time evolution of these configurations is in qualitative agreement with perturbation theory and the spherical collapse model.

The question we addressed is whether the luminosity distance of a light source may increase in such a background. We found that this is indeed possible. If the inhomogeneities involve a central underdensity and an overdense outer shell, the luminosity distance is larger on the average than if the matter was distributed homogeneously. The opposite happens if the inhomogeneity is denser in the middle, surrounded by an underdense shell. In this case the luminosity distance is smaller than in homogeneous cosmology. These results imply that a description of the Universe as being composed of large voids, with the matter being concentrated in the intermediate regions, could provide a basis for the explanation of the supernova data without dark energy.

The problem with the picture emerging from our model is quantitative: The increase in the luminosity distance arising from void domination is too small to account for the supernova data. The relative increase at a redshift around 1 is of the order of a few %. Moreover, an absolute upper bound of around 10% can be derived. This is significantly smaller than the required increase, which is around 30%.

We mention at this point that in our model the change in redshift because of the presence of inhomogeneities is smaller than the change in luminosity distance by more than an order of magnitude. As a result, we do not expect a large Rees-Sciama effect [26] that would be in conflict with the CMB data. It is also possible that the presence of voids could explain the observed large angle CMB anomalies [34].

The open question is whether an alternative model of large scale structure could result in a larger effect. There is a variety of metrics describing inhomogeneous cosmologies, so this cannot be excluded. In our modelling we have made some fundamental assumptions

that limit the possibilities. These are:

- a) The overall scale factor is determined by the average density through the standard Friedmann equation.
- b) The observer does not occupy a preferred position in the Universe, such as the center of a significant underdensity. In practice, we studied light signals that originate in a homogeneous region, cross a large number of inhomogeneities, and are detected by an observer within a homogeneous region.
- c) The inhomogeneities have a characteristic scale $\mathcal{O}(10) h^{-1}$ Mpc today. Their evolution is consistent with the standard theory of structure formation. In particular, the density perturbations are $\mathcal{O}(10^{-5})$ at horizon crossing.

The first two assumptions lead to the LTB Swiss-cheese model that we studied. The third one is consistent with the observed size of voids in the matter distribution of the Universe.

If the first assumption is maintained we do not expect a significant increase of the luminosity distance, independently of the modelling of the inhomogeneous regions. The analytical upper bound of approximately 10% at redshifts around 1 would remain valid in all such cosmologies, as long as the overall scale factor is determined by the average density through the standard Friedmann equation.

Of course, one could try to build a cosmology that deviates significantly from the FRW one, so that the effective Friedmann equation receives large corrections. An important limitation is that acceleration of the local volume expansion in the absence of vorticity requires $\rho + 3p < 0$, with ρ the local energy density and p the pressure [5].

It has been suggested that the average expansion rate in a given background may deviate from the local one, with the corrections accounting for the observed acceleration [6, 12, 30, 31]. However, how the averaging is reflected in the features of a light beam transmitted in the particular background is not clear yet. Obviously the light propagates within the exact local metric, for which the optical equations lead to an unambiguous determination of the luminosity distance. On the other hand, the notion of averaging becomes crucial for a complicated mass distribution, for which the exact local metric cannot be determined. In this case the averaging should be a method of determining the gross features of light propagation without considering all the details of the exact metric. More work is needed in order to have a clear understanding of the connection between averaging and beam features. For example, within our model the “backreaction” term appearing in the averaged Raychaudhuri equation [30] is zero. Despite that, we observe a modification of the luminosity distance.

The basic features required for the averaging to induce a significant deviation from the standard Friedmann expansion were determined recently [32]. The average spatial curvature plays an important role in this respect, as it is coupled to large spatial variances of the local expansion rate and shear. Within our model the average spatial curvature is zero, so that this mechanism of “backreaction” through averaging is absent. This is

a consequence of the initial conditions we chose for the LTB metric. As we discussed in section 3, our initial conditions guarantee that the evolution of the inhomogeneities is consistent with the standard scenario of structure formation (our third assumption). Maintaining this consistency in backgrounds with large average spatial curvature (similar to those proposed in refs. [15, 16]) is a challenging problem that merits further study in the future. An exact background that preserves this consistency could help test the proposal of “backreaction” through averaging, by studying the exact light propagation in it.

Another possibility in order to explain the supernova data is to violate our second assumption and place the observer in a special position in the Universe. It has been observed that any form of the luminosity distance as a function of redshift can be reproduced for an observer at the center of the LTB metric [9]. The reason is that, within an anisotropic geometry, the volume expansion rate results from the averaging of unequal expansion rates along various directions. In particular, for the LTB metric the radial expansion can be accelerating, while the tangential one decelerating [17]. Of course, the local volume expansion is always decelerating for $\rho + 3p > 0$. An observer located at the center of the LTB metric receives signals only along the radial direction, from which he may infer an accelerating expansion.

Reproducing the supernova data in LTB models requires a variation of the density or the expansion rate over distances $\mathcal{O}(10^3) h^{-1}$ Mpc [14]–[18] (also see [33]). This implies inhomogeneities at scales much larger than the ones allowed by our third assumption. Moreover, in order to avoid a conflict with the isotropy of the CMB, the location of the observer must be very close to the center of the spherical configuration described by the LTB metric. Typically the required density contrast is of order $\mathcal{O}(1)$. A notable exception is discussed in ref. [15]. In the model presented there, the matter distribution is homogeneous, but the expansion rate varies by roughly 15% over distances $\mathcal{O}(10^3) h^{-1}$ Mpc. This results from a variation of the spatial curvature. Even though the conflict with the observed matter distribution is avoided in this way, the lack of consistency with the theory of structure formation and the requirement of a preferred location of the observer are the weak points of this approach.

In all the models that reproduce the supernova data by placing the observer at the center of the LTB geometry the Universe is very inhomogeneous at earlier times. The problem of initial conditions remains open, while the consistency with the amplitude of the temperature fluctuations of the CMB is not obvious. In our approach we constrained our modelling of the inhomogeneities so that it leads to consistency with the theory of structure formation. Our findings indicate that the constraints do not permit the reproduction of the supernova data without dark energy.

It is worth pointing out that the model we considered has zero vorticity. The presence of vorticity in the background geometry gives a positive contribution to the expansion of

the beam area [22]. Such models are difficult to study, but provide another unexplored possibility for the explanation of the supernova luminosity distance without dark energy.

As a final remark we mention that the effect we studied in this work is important for the correct determination of the energy content of the Universe. Even in the presence of dark energy, the corrections to the luminosity distance arising from inhomogeneities must be taken into account, as they can modify significantly the deduced contributions from dark matter and dark energy to the total energy density [28].

Acknowledgments

We would like to thank S. Rasanen for useful discussions and comments. This work was supported by the research program “Pythagoras II” (grant 70-03-7992) of the Greek Ministry of National Education, partially funded by the European Union.

8. Appendix A

For completeness, we derive in this appendix the optical equations in a form that is convenient for our study. We follow closely the presentation in ref. [22].

The equation for the deviation between two neighboring null geodesics $x^i(\lambda)$ and $x^i(\lambda) + \xi^i(\lambda)$ is

$$\frac{D^2\xi^i}{d\lambda^2} = R^i_{\ jkl}k^j k^k \xi^l. \quad (8.1)$$

The symbol D denotes a covariant derivative, while λ is an affine parameter. A null geodesic is defined through the relations

$$k^i = \frac{dx^i}{d\lambda}, \quad k^i_{\ ;j} k^j = 0, \quad k^i k_i = 0. \quad (8.2)$$

We are interested in finding a pseudo-orthonormal basis of vectors along the path of light, in which we can describe the evolution of the cross section of a beam of light. As such we use k^i , a null vector w^i satisfying $w^i k_i = -1$, and L_1^i, L_2^i , which are space-like unit vectors, orthogonal to the light ray and to each other. We require that all these be parallelly propagated along the path, so as to keep them orthogonal and normalized. In summary, we have along the path

$$kk = ww = 0, \quad L_1 L_1 = L_2 L_2 = 1, \quad kw = -1, \quad (8.3)$$

$$kL_1 = kL_2 = wL_1 = wL_2 = L_1 L_2 = 0. \quad (8.4)$$

We can choose the initial deviation ξ^i such that a freely moving observer sees it perpendicular to the light ray: $k_i \xi^i = 0$, $w_i \xi^i = 0$. It is easy then to check that the deviation remains orthogonal to the rest of the path. As a result, ξ^i can be expressed as a linear combination of the vectors L_a^i

$$\xi^i(\lambda) = \sum_{a=1,2} d_a(\lambda) L_a^i, \quad (8.5)$$

where the scalars d_a are the proper orthogonal components of the separation of the two light rays. Substituting this expansion into eq. (8.1) and using the orthogonality of L_a^i , we get

$$\frac{d^2 d_a}{d\lambda^2} = \sum_b A_{ab} d_b, \quad A_{ab} = R_{ijkl} L_a^i k^j k^k L_b^l. \quad (8.6)$$

The decomposition of the curvature tensor into the Ricci and Weyl tensors

$$R_{ijkl} = \frac{1}{2} (g_{ik} R_{jl} - g_{il} R_{jk} - g_{jk} R_{il} + g_{jl} R_{ik}) - \frac{1}{6} (g_{ik} g_{jl} - g_{il} g_{jk}) R + C_{ijkl}$$

gives

$$A_{ab} = -\frac{1}{2} R_{ij} k^i k^j \delta_{ab} + C_{ijkl} L_a^i k^j k^k L_b^l. \quad (8.7)$$

The components d_a obey the equation

$$\frac{dd_a}{d\lambda} = \sum_b (\theta \delta_{ab} + \sigma_{ab}) d_b, \quad (8.8)$$

where θ is the expansion of the beam and σ_{ab} the symmetric and traceless shear tensor

$$\sigma_{ab} = \begin{pmatrix} \sigma_1 & \sigma_2 \\ \sigma_2 & -\sigma_1 \end{pmatrix}. \quad (8.9)$$

The later satisfies

$$\sum_c \sigma_{ac} \sigma_{cb} = (\sigma_1^2 + \sigma_2^2) \delta_{ab} = \sigma^2 \delta_{ab}. \quad (8.10)$$

The second derivative of eq. (8.8) implies that

$$A_{ab} = \left(\frac{d\theta}{d\lambda} + \theta^2 + \sigma^2 \right) \delta_{ab} + \left(\frac{d\sigma_{ab}}{d\lambda} + 2\theta\sigma_{ab} \right). \quad (8.11)$$

Using the identity $\sum_a C_{ijkl} L_a^i k^j k^k L_a^l = 0$, we can see that the second term of (8.7) is traceless, as is the second term of (8.11). We have then

$$\frac{d\theta}{d\lambda} + \theta^2 + \sigma^2 = -\frac{1}{2} R_{ij} k^i k^j \quad (8.12)$$

$$\frac{d\sigma_{ab}}{d\lambda} + 2\theta\sigma_{ab} = C_{ijkl} L_a^i k^j k^k L_b^l. \quad (8.13)$$

The components d_a at neighboring positions along the path are

$$\bar{d}_a \equiv d_a(\lambda + \delta\lambda) = d_a(\lambda) + \left(\theta d_a + \sum_b \sigma_{ab} d_b \right) \delta\lambda. \quad (8.14)$$

The proper cross-section area A of the beam at neighboring positions along the path is

$$A(\lambda + \delta\lambda) = \int d\bar{d}_1 d\bar{d}_2 = \int dd_1 dd_2 \frac{\partial \bar{d}}{\partial d} = \frac{\partial \bar{d}}{\partial d} A(\lambda). \quad (8.15)$$

Evaluating the Jacobian $\partial \bar{d}/\partial d$ results in

$$\frac{dA}{d\lambda} = 2\theta A. \quad (8.16)$$

Eqs. (8.12) and (8.13) can now be written as

$$\frac{1}{\sqrt{A}} \frac{d^2 \sqrt{A}}{d\lambda^2} + \sigma^2 = -\frac{1}{2} R_{ij} k^i k^j \quad (8.17)$$

$$\frac{d(A\sigma_{ab})}{d\lambda} = A C_{ijkl} L_a^i k^j k^k L_b^l. \quad (8.18)$$

In this work we study light propagation in space-times with spherical spatial symmetry. In such cases, the off-diagonal elements σ_2 of the shear tensor can be set consistently to zero. The reason is that the eigenvalues $\pm\sigma$ of the shear tensor determine the deformation of a surface along two principal orthogonal axes perpendicular to the light direction. The rate of stretching in these two directions is given by $\theta + \sigma$ and $\theta - \sigma$,

respectively. The off-diagonal elements σ_2 are related to the orientation of the principal axes with respect to the space-like unit vectors L_1^i, L_2^i . In the case of spherical symmetry, one principal axis lies on the plane determined by the null geodesic and the center of symmetry and the second perpendicularly to it. It is possible then to take L_1^i, L_2^i along the principal directions. This leads to $\sigma_2 = 0$, which is equivalent to $C_{ijkl}L_1^i k^j k^k L_2^l = 0$. We have checked explicitly that this condition is satisfied for all the space-times we consider in this work. As a result, eq. (8.13) becomes

$$\frac{d\sigma}{d\lambda} + 2\theta\sigma = C_{ijkl}L_1^i k^j k^k L_1^l, \quad (8.19)$$

and eq. (8.18)

$$\frac{d(A\sigma)}{d\lambda} = AC_{ijkl}L_1^i k^j k^k L_1^l. \quad (8.20)$$

The basic optical equations for our study are eqs. (8.12), (8.19), or equivalently eqs. (8.17), (8.20).

9. Appendix B

In the appendix we derive the form of the optical equations (8.16)–(8.20) in specific backgrounds.

9.1. Lemaitre-Tolman-Bondi (LTB) background

A pseudo-orthonormal basis of vectors along a null geodesic is

$$k = (k^0, k^1, 0, k^3) \quad (9.1)$$

$$L_1 = \left(0, 0, \frac{1}{R}, 0\right) \quad (9.2)$$

$$L_2 = \left(\frac{hk^0R + k^1b}{k^3R}, \frac{k^0 + hRk^1b}{k^3bR}, 0, h\right) \quad (9.3)$$

$$w = \left(\frac{k^0 + hR(2k^1b + hk^0R)}{2(k^3)^2 R^2}, \frac{k^1b(h^2R^2 + 1) + 2hk^0R}{2(k^3)^2 bR^2}, 0, \frac{h^2R^2 - 1}{2k^3R^2}\right) \quad (9.4)$$

where the function $h(r, t, u)$ is arbitrary. For these vectors to be parallelly propagated along the light path, the function h must satisfy the differential equation

$$\frac{dh}{d\lambda} = -\frac{1}{R^2b} \left[2bhR \left(\dot{R}k^0 + R'k^1 \right) + \dot{R}b^2k^1 + k^0R' \right].$$

The explicit form of the solution is not necessary for our purposes, as the quantities

$$R_{ij}k^i k^j = \frac{1}{2M^2}\rho(k^0)^2 \quad (9.5)$$

$$C_{ijkl}L_1^i k^j k^k L_1^l = \frac{(k^3)^2}{4M^2R^2} \left(\rho - \frac{3\mathcal{M}(r)}{4\pi R^3} \right) \quad (9.6)$$

$$C_{ijkl}L_1^i k^j k^k L_2^l = 0 \quad (9.7)$$

do not depend on h . As remarked in the previous appendix, we can set $\sigma_2 = 0$. The evolution of the expansion θ and the shear $\sigma = \sigma_1$ of a beam is given by eqs. (2.14), (2.15) while the beam area evolves according to eq. (2.16).

9.2. Schwarzschild background

A pseudo-orthonormal basis of vectors along a null geodesic is

$$k = (k^0, k^1, 0, k^3) \quad (9.8)$$

$$L_1 = \left(0, 0, \frac{1}{r}, 0\right) \quad (9.9)$$

$$L_2 = \left(\frac{hk^0}{k^3} + \frac{k^1}{k^3 r} \left(1 - \frac{r_s}{r}\right)^{-1}, \frac{hk^1}{k^3} + \frac{k^0}{k^3 r} \left(1 - \frac{r_s}{r}\right), 0, h\right) \quad (9.10)$$

$$w = \frac{1}{2(k^3)^2 r^2} \left(k^0 \left(h^2 r^2 + 1 \right) + 2h r k^1 \left(1 - \frac{r_s}{r} \right)^{-1}, \right. \\ \left. k^1 \left(h^2 r^2 + 1 \right) + 2h r k^0 \left(1 - \frac{r_s}{r} \right), 0, k^3 \left(h^2 r^2 - 1 \right) \right), \quad (9.11)$$

where the function $h(r, t, u)$ is arbitrary. For these vectors to be parallelly propagated along the light path, the function h must satisfy the differential equation

$$\frac{dh}{d\lambda} + 2\frac{hk^1}{r} + \frac{k^0}{r^2} \left(1 - \frac{r_s}{r}\right) = 0.$$

We have

$$R_{ij} k^i k^j = 0 \quad (9.12)$$

$$C_{ijkl} L_1^i k^j k^k L_1^l = -\frac{3(k^3)^2}{2} \frac{r_s}{r} \quad (9.13)$$

$$C_{ijkl} L_1^i k^j k^k L_2^l = 0, \quad (9.14)$$

and we can set $\sigma_2 = 0$. The evolution of the expansion θ and the shear $\sigma = \sigma_1$ of a beam is given by eqs. (2.35), (2.36) while the beam area evolves according to eq. (2.37).

References

- [1] A. G. Riess *et al.* [Supernova Search Team Collaboration], *Astron. J.* **116** (1998) 1009 [arXiv:astro-ph/9805201]; *Astrophys. J.* **607** (2004) 665 [arXiv:astro-ph/0402512];
S. Perlmutter *et al.* [Supernova Cosmology Project Collaboration], *Astrophys. J.* **517** (1999) 565 [arXiv:astro-ph/9812133].
- [2] W. J. Percival *et al.* [The 2dFGRS Collaboration], *Mon. Not. Roy. Astron. Soc.* **327** (2001) 1297 [arXiv:astro-ph/0105252];
J. L. Sievers *et al.*, *Astrophys. J.* **591** (2003) 599 [arXiv:astro-ph/0205387].
- [3] D. N. Spergel *et al.* [WMAP Collaboration], *Astrophys. J. Suppl.* **148** (2003) 175 [arXiv:astro-ph/0302209].
- [4] E. W. Kolb, S. Matarrese, A. Notari and A. Riotto, arXiv:hep-th/0503117;
P. Martineau and R. Brandenberger, arXiv:astro-ph/0510523.
- [5] C. M. Hirata and U. Seljak, *Phys. Rev. D* **72** (2005) 083501 [arXiv:astro-ph/0503582];
C. Wetterich, *Phys. Rev. D* **67** (2003) 043513 [arXiv:astro-ph/0111166];
G. Geshnizjani, D. J. H. Chung and N. Afshordi, *Phys. Rev. D* **72** (2005) 023517 [arXiv:astro-ph/0503553];
E. E. Flanagan, *Phys. Rev. D* **71** (2005) 103521 [arXiv:hep-th/0503202].
- [6] S. Rasanen, *Class. Quant. Grav.* **23** (2006) 1823 [arXiv:astro-ph/0504005].
- [7] S. Rasanen, *JCAP* **0402** (2004) 003 [arXiv:astro-ph/0311257];
E. W. Kolb, S. Matarrese, A. Notari and A. Riotto, *Phys. Rev. D* **71** (2005) 023524 [arXiv:hep-ph/0409038].
- [8] G. Lemaitre, *Gen. Rel. Grav.* **29** (1997) 641;
R. C. Tolman, *Proc. Nat. Acad. Sci.* **20** (1934) 169;
H. Bondi, *Mon. Not. Roy. Astron. Soc.* **107** (1947) 410.
- [9] N. Mustapha, C. Hellaby and G. F. R. Ellis, *Mon. Not. Roy. Astron. Soc.* **292** (1997) 817 [arXiv:gr-qc/9808079].
- [10] M. N. Celerier, *Astron. Astrophys.* **353** (2000) 63 [arXiv:astro-ph/9907206].
- [11] H. Iguchi, T. Nakamura and K. i. Nakao, *Prog. Theor. Phys.* **108** (2002) 809 [arXiv:astro-ph/0112419];
K. Bolejko, arXiv:astro-ph/0512103;
R. Mansouri, arXiv:astro-ph/0512605;
R. A. Vanderveld, E. E. Flanagan and I. Wasserman, *Phys. Rev. D* **74** (2006) 023506 [arXiv:astro-ph/0602476];
D. Garfinkle, *Class. Quant. Grav.* **23** (2006) 4811 [arXiv:gr-qc/0605088];
D. J. H. Chung and A. E. Romano, *Phys. Rev. D* **74** (2006) 103507 [arXiv:astro-ph/0608403].
- [12] S. Rasanen, *JCAP* **0411** (2004) 010 [arXiv:gr-qc/0408097]; *JCAP* **0611** (2006) 003 [arXiv:astro-ph/0607626].
- [13] J. W. Moffat, *JCAP* **0510** (2005) 012 [arXiv:astro-ph/0502110]; arXiv:astro-ph/0505326.
- [14] H. Alnes, M. Amarzguioui and O. Gron, arXiv:astro-ph/0506449; *Phys. Rev. D* **73** (2006) 083519 [arXiv:astro-ph/0512006];
H. Alnes and M. Amarzguioui, arXiv:astro-ph/0610331.
- [15] K. Enqvist and T. Mattsson, arXiv:astro-ph/0609120.
- [16] C.-H. Chuang, J.-A. Gu and W.-Y. P. Hwang, arXiv:astro-ph/0512651.
- [17] P. S. Apostolopoulos, N. Brouzakis, N. Tetradis and E. Tzavara, *JCAP* **0606** (2006) 009 [arXiv:astro-ph/0603234].
- [18] T. Biswas, R. Mansouri and A. Notari, arXiv:astro-ph/0606703.
- [19] A. Einstein and E. G. Straus, *Rev. Mod. Phys.* **17** (1945) 120; *ibid.* **18** (1946) 148.

- [20] R. K. Sachs, Proc. Roy. Soc. London A **264** (1961) 309.
- [21] R. Kantowski, Astrophys. J. **155** (1969) 89.
- [22] S. W. Hawking and G. F. R. Ellis, *The Large Scale Structure of Space-Time*, Cambridge University Press, Cambridge;
P. J. E. Peebles, *Principles of Physical Cosmology*, Princeton University Press, Princeton.
- [23] P. Schneider, J. Ehlers and E. E. Falco, *Gravitational Lenses*, Springer-Verlag, Berlin.
- [24] J. E. Gunn and J. R. I. Gott, Astrophys. J. **176**, 1 (1972);
A. Cooray and R. Sheth, Phys. Rept. **372** (2002) 1 [arXiv:astro-ph/0206508].
- [25] K. Bolejko, A. Krasinski and C. Hellaby, Mon. Not. Roy. Astron. Soc. **362** (2005) 213 [arXiv:gr-qc/0411126];
C. Hellaby and A. Krasinski, Phys. Rev. D **73** (2006) 023518 [arXiv:gr-qc/0510093].
- [26] M. J. Rees and D. W. Sciama, Nature **217** (1968) 511.
- [27] C. C. Dyer and R. C. Roeder, Astrophys. J. **174**, L115 (1972); *ibid.* **180**, L31 (1973).
- [28] R. Kantowski, Astrophys. J. **507** (1998) 483 [arXiv:astro-ph/9802208]; Phys. Rev. D **68** (2003) 123516 [arXiv:astro-ph/0308419];
R. Kantowski and R. C. Thomas, Astrophys. J. **561** (2001) 491 [arXiv:astro-ph/0011176].
- [29] Ya. B. Zel'dovich, Soviet. Astr. – AJ **8** (1964) 64;
V. M. Dashevskii and V. I. Slysh, Soviet. Astr. – AJ **9** (1966) 671.
- [30] T. Buchert, Gen. Rel. Grav. **32** (2000) 105 [arXiv:gr-qc/9906015];
Gen. Rel. Grav. **33** (2001) 1381 [arXiv:gr-qc/0102049].
- [31] Y. Nambu and M. Tanimoto, arXiv:gr-qc/0507057;
A. Paranjape and T. P. Singh, Class. Quant. Grav. **23** (2006) 6955 [arXiv:astro-ph/0605195];
arXiv:astro-ph/0609481;
A. E. Romano, arXiv:astro-ph/0612002.
- [32] T. Buchert, Class. Quant. Grav. **23** (2006) 817 [arXiv:gr-qc/0509124];
T. Buchert, J. Larena and J. M. Alimi, Class. Quant. Grav. **23** (2006) 6379 [arXiv:gr-qc/0606020].
- [33] K. Tomita, Astrophys. J. **529**, 26 (2000); Astrophys. J. **529**, 38 (2000); Mon. Not. Roy. Astron. Soc. **326** (2001) 287 [arXiv:astro-ph/0011484].
- [34] K. T. Inoue and J. Silk, arXiv:astro-ph/0602478; arXiv:astro-ph/0612347.